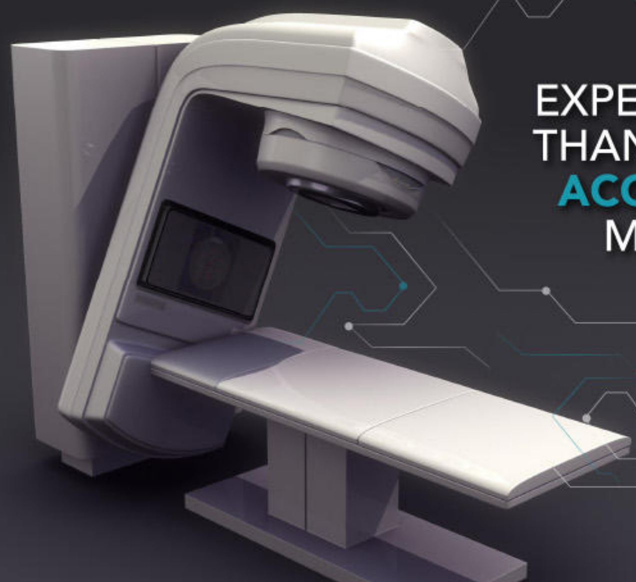

EXPECT NOTHING LESS THAN SUB-MILLIMETER ACCURACY IN YOUR MEASUREMENTS

START UTILIZING ADVANCED PRECISION QA TODAY

THE RIT FAMILY OF PRODUCTS **VERSION 6.7.X**

3D Winston-Lutz Isocenter Optimization

The enhanced isocenter optimization routine allows for optimal cone detection, resulting in the utmost precision. The accuracy of this routine now surpasses sub-millimeter resolution. *(Pictured above)*

Cerberus 2.0: The Future of Complete Automation

Completely streamline your automated phantom analysis workflow with the new Cerberus. Cerberus operates in the background of your workstation, allowing for hands-free Imaging QA.

One-Click, Instant Automated Phantom Analyses

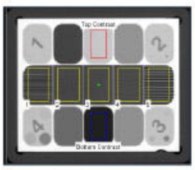

RIT's full suite of phantom analyses provides fast, robust, and accurate analysis of all imaging tests recommended in TG-142. The software now offers added support for the QCkV-1 phantom. *(Pictured right)*

Tolerance Customization and Management

RIT's new Tolerance Manager offers comprehensive customization of tolerance values for every measurement used in all automated phantom analyses. Tolerance profiles can be precisely-tailored to each individual machine in use.

CLICK HERE TO DOWNLOAD TODAY

Elekta Leaf Speed Analysis

RIT now offers fast and accurate automated analysis for Elekta MLC QA. The new Leaf Speed Analysis routine measures the consistency and accuracy of the MLC leaf speeds as they traverse the imager.

TomoTherapy® Registration for Patient QA

Easily perform exact dose comparisons with RIT's new TomoTherapy Registration routine. This new, innovative wizard uses a TomoTherapy® plan, dose map, and a film to determine position an dose accuracy using the red lasers. *(Pictured below)*

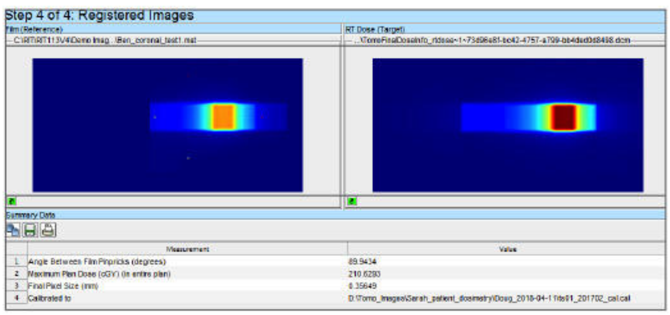

Streamline Your QA Workflow

Fully-customize your software experience with RIT's updated and dynamic interface. With the new ability to hide/display any features or sections, you can instantly access you most frequently-performed analysis routines.

Convenient, Cloud-Based Software Licensing

Easily manage your software licenses with RIT's new, flexible system at your convenience, 24/7/365 without the help of RIT Technical Support. Upgrading is now easier than ever.

RADIOLOGICAL IMAGING TECHNOLOGY, INC.
RADIMAGE.COM
(+1) 719.590.1077 x211 // sales@radimage.com
Connect with RIT @RIT4QA

Systematic study on factors influencing the performance of interdetector scatter recovery in small-animal PET

Seungeun Lee
Department of Biomedical Sciences, Seoul National University College of Medicine, Seoul 03080, Korea
Department of Nuclear Medicine, Seoul National University College of Medicine, Seoul 03080, Korea

Min Sun Lee
Department of Nuclear Medicine, Seoul National University College of Medicine, Seoul 03080, Korea
Interdisciplinary Program in Radiation Applied Life Science, Seoul National University, Seoul 03080, Korea

Kyeong Yun Kim
Department of Biomedical Sciences, Seoul National University College of Medicine, Seoul 03080, Korea
Department of Nuclear Medicine, Seoul National University College of Medicine, Seoul 03080, Korea

Jae Sung Lee[a)]
Department of Biomedical Sciences, Seoul National University College of Medicine, Seoul 03080, Korea
Department of Nuclear Medicine, Seoul National University College of Medicine, Seoul 03080, Korea
Interdisciplinary Program in Radiation Applied Life Science, Seoul National University, Seoul 03080, Korea
Institute of Radiation Medicine, Medical Research Center, Seoul National University, Seoul 03080, Korea

(Received 29 December 2017; revised 11 May 2018; accepted for publication 13 May 2018; published 22 June 2018)

Purpose: Interdetector scatter (IDS) is a triple coincidence caused by the Compton scatter of an annihilation photon from one detector block to another which frequently occurs in small-animal positron emission tomography (PET). By finding the true lines-of-response (LORs) of annihilation photon pairs among three possible LORs in IDS events, we can utilize these recovered events to improve the sensitivity of PET systems. IDS recovery should be accurate to yield reliable images with relatively short scan times. We systemically investigated physical factors affecting IDS recovery performance, focusing on the reconstructed image quality of small-animal PET. We evaluated sensitivity increase, recovery accuracy, and image quality by applying different combinations of energy window, recovery scheme, and scanner properties.

Methods: We used GATE Monte Carlo simulation to acquire coincidence events from a NEMA NU 4-2008 image quality phantom using small-animal PET scanner with axial field of view of 55 mm and diameter of 64 mm. We first defined energy window criteria to obtain valid IDS events. Their role was to assign triple coincidences as IDS events and to restrict the number of LOR candidates to two. We tested three different energy windows around 511 keV. Second, we applied four different recovery schemes (maximum energy, Compton kinematics, neural network, and proportional) to assigned IDS events. To measure the effects of scanner properties, energy resolutions of 0–20% and one to four depth-of-interaction (DOI) layers were simulated. For every combination of the factors, we measured sensitivity increase and recovery accuracy. We also analyzed the reconstructed images for each IDS recovery method in terms of mean pixel intensity, noise, signal-to-noise ratio (SNR), contrast, and recovery coefficients.

Results: Sensitivity increase depended on the energy window and energy resolution. The maximum increase in sensitivity was 33% when energy window of [250, 750] keV was applied. Higher energy resolution yielded larger sensitivity increase, especially for narrow windows. Recovery accuracy was affected by all the factors tested in this study. Accuracy increased with narrower energy window, and a neural network scheme was the most accurate. The better energy resolution and DOI capability improved accuracy by providing precise measurement of energies and interaction positions. In image quality analysis, noise and SNR were highly dependent on the sensitivity increase and energy window. When the same energy window was applied, SNR, contrast, and recovery coefficients were higher with higher accuracy of the scheme. Meanwhile, the proportional scheme yielded the best image quality among the schemes and reduced 20% of scan time to achieve the same SNR as that of double coincidence images.

Conclusions: As a fundamental research for real implementation of IDS recovery, we conducted a simulation study to evaluate the factors affecting sensitivity increase, recovery accuracy, and image quality. Sensitivity increase was dependent on the energy window and energy resolution, while the recovery accuracy was affected by energy window, recovery scheme, energy resolution, and DOI capability. In image quality analysis, sensitivity increase and recovery accuracy dominantly affected the noise and quantitative accuracy, respectively. Among the recovery schemes, the proportional scheme obtained the best image quality. [https://doi.org/10.1002/mp.13020]

Key words: interdetector scatter, PET

1. INTRODUCTION

Positron emission tomography (PET) is a useful imaging tool for clinical diagnosis and medical research.[1–3] Sensitivity is one of the major performance factors of PET scanners. The high sensitivity of PET makes it possible to achieve high signal-to-noise ratios (SNRs) and thus enhances lesion detectability with relatively short scan time and low administered dose. There are various strategies for the improvement of PET sensitivity. One strategy is to alter the PET scanner geometry to increase detectable events by extending field of view[4–8] and using long scintillation crystals.[6–9] Implementation of the time-of-flight technologies that localize line-of-responses (LORs) with time differences in annihilation photon pair arrivals[10–12] is also a powerful strategy. Therefore, the technologies for enhancing the time resolution of PET are actively being investigated.[13–15] Moreover, use of single-photon events with Compton imaging has been suggested.[16–18]

Recovering triple coincidences has been proposed as another approach for sensitivity increase.[19,20] Typically in PET imaging, a pair of 511-keV annihilation photons are coincidently detected and a (LOR) is drawn. Triple coincidence is defined as an event in which photons are detected at three detector blocks coincidently in PET. Interdetector scatter (IDS) and random triple (RNT) are major types of triple coincidence. IDS is caused by the Compton scatter of one annihilation photon from a detector block to an adjacent one as shown in Fig. 1(a). It accounts for a large proportion of multiple coincidences especially in a small-animal PET scanner because of the small size of the crystal arrays. RNT occurs by coincident detection of a pair of annihilation photons along with a single photon or three single photons. LORs of double coincidences are used for histogram or sinogram generation, but the multiple coincidences are practically rejected in most preclinical and clinical PET scanners. The purpose of IDS recovery is to accurately find the true LOR drawn along the first interacted positions of IDS events and include them in data for image reconstruction. When implementing IDS recovery, it is important not only to maximize the number of IDS events for recovery but also to optimize accuracy as well as image quality.

However, the factors that affect IDS recovery performance focusing on reconstructed PET image quality have not been systematically investigated. Therefore, in this study, we evaluated the factors of IDS recovery performance in a small-animal PET scanner with Monte Carlo simulation. First, we tested different energy criteria for triple coincidence for IDS validation because they are likely to determine the number of IDS events to be recovered. Second, we compared different recovery schemes that are expected to be efficient for small-animal PET geometry and relatively simple for real implementation.[21–24] An accurate recovery scheme has to be applied to correctly find the true LORs of the IDS events.[20,25–28] Finally, the effects of the PET system properties, including energy resolution and DOI capabilities on the performance of IDS recovery methods were explored. We measured sensitivity increase and IDS recovery accuracy for evaluation, and analyzed the effects of IDS recovery methods on image quality.

2. MATERIALS AND METHODS

2.A. Simulation setup

We used a GATE Monte Carlo simulation toolkit (v.7.0) for the application and evaluation of the recovery methods.[29] The simulated scanner was our preclinical PET, which has the same physical properties of SimPET (Brightonix Imaging Inc., Seoul, Korea) used for a hybrid PET/MR imaging (Fig. 2). The main properties of SimPET are summarized in Table I, and further details are described in Ko, Kim et al.[30] and Ko, Yoon et al.[31] For the digitizer settings in GATE, we used a coincidence time window of 12 ns. In addition, a multiple coincidence sorter was set to *takeAllGoods* assuming that the system is able to record all of the multiple coincidences.

The phantom used for imaging was a NEMA NU 4-2008 image quality phantom[32] which was composed of uniform, hot, cold, and rod regions [Figs. 2(a) and 2(b)]. To evaluate SNR and to clearly show the effects of IDS recovery, the activity distribution was modified to be 1:2.5 in uniform and hot regions. The rod region consisted of five rods with diameters of 1–5 mm arranged in a circle. The total activity of 511-keV back-to-back source inside the phantom was 3.7×10^6 Bq, and the default acquisition time was set to 10 min. Additionally, the list-mode data for the simulated 10-min total acquisition was rebinned into 1-, 2-, ...10-min acquisitions to examine the dependency of SNR on acquisition time for every recovery scheme.

2.B. Energy windows for IDS assigning criteria

In GATE simulation, the types of coincidence and the types of radiation interaction of detected events are recorded as outputs. In real PET scanners, however, it is unknown whether a triple coincidence is an IDS and whether an interaction is photoelectric absorption or Compton scatter. Therefore, certain criteria for assigning IDS events should be established prior to application of recovery schemes.

When a triple coincidence occurred in three detector blocks as shown in Fig. 1(b), a position with the largest energy deposition was assumed to be where a single

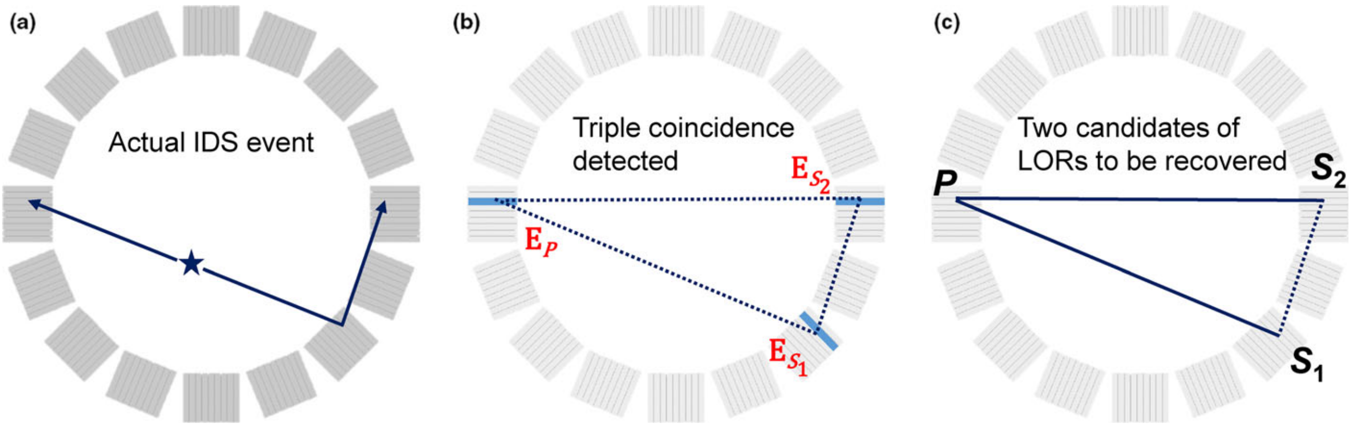

FIG. 1. Example of an IDS event in a PET scanner. (a) Actual IDS scenario. (b) Detection of triple coincidence in case of (a). Deposited energies are labeled as E_P for the largest and E_{S1} and E_{S2} for others. (c) After the event was assigned as an IDS, PS_1 and PS_2 were used for the recovery. [Color figure can be viewed at wileyonlinelibrary.com]

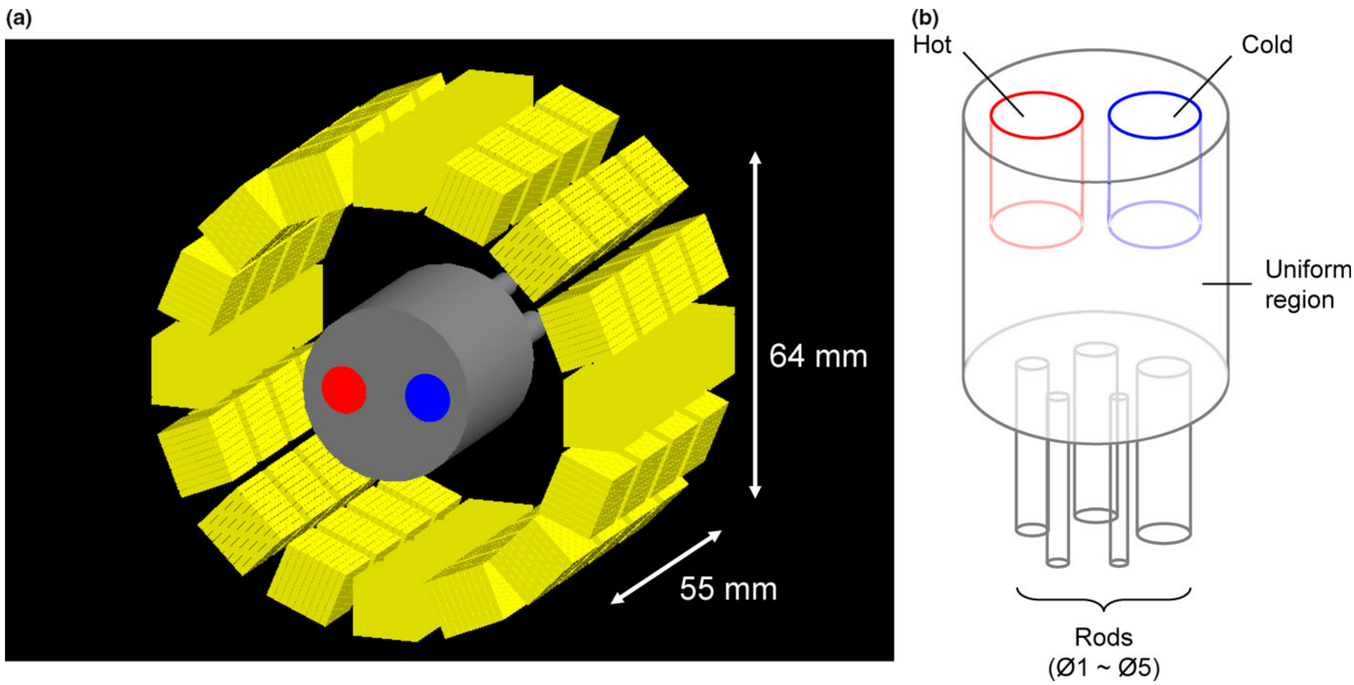

FIG. 2. GATE-simulated geometries. (a) PET scanner (SimPET) and NEMA NU 4-2008 image quality phantom. The activity concentration ratio between the uniform, hot, and cold regions was 1:2.5:0. (b) Schema of NEMA NU 4-2008 image quality phantom containing hot, cold, uniform, and rod regions. [Color figure can be viewed at wileyonlinelibrary.com]

TABLE I. Main properties of simulated PET.

Property	Setting
Crystal material	LSO (Lu_2SiO_5)
Crystal size (mm^3)	1.2 × 1.2 × 10
Crystal density (g/cm^3)	7.4
Number of crystals per block	9 × 9
Number of blocks per ring	16
Number of rings	4
Axial FOV (mm)	55
Ring diameter (mm)	64

photoelectric absorption of an unscattered photon occurred. Two other positions were assumed to be where Compton-scattered photons interacted. The positions were labeled as P for photoelectric absorption, and S_1 and S_2 for scattered photon detection. To assign a triple coincidence as an IDS, deposited energies of the triple coincidence are required to meet the criteria presented in Eqs. (1) and (2).

$$E_{low} < E_P < E_{up} \tag{1}$$

$$E_{low} < E_{S_1} + E_{S_2} < E_{up} \tag{2}$$

After assignment from the *Coincidence* output file, we can regard PS_1 and PS_2 as the candidates for the true LOR

[Fig. 1(c)]. We applied three different energy windows, [E_{low}, E_{up}] = [250, 750] keV, [350, 650] keV, and [450, 550] keV, to IDS data. The width of the energy window is not only related to the number of usable IDS events for recovery but also the accuracy of IDS recovery, because it determines the validity of triple coincidence as an IDS event. To investigate the efficiency of the energy criteria, we defined "valid IDS ratio" as the ratio of valid IDS events to total assigned IDS events. Here, a valid IDS event is a triple coincidence that meets all the following three criteria: (a) the triple coincidence is an IDS event, (b) P is the position of photoelectric absorption and (c) S_1 and S_2 are the positions of Compton-scattered photons interacted. The valid IDS ratio was measured through the *Hits* output file of GATE.

2.C. Recovery schemes

2.C.1. Maximum energy scheme

The maximum energy (ME) scheme simply selected a first interaction position where greater energy was deposited between S_1 and S_2.[21,25] The detected IDS events in our PET system were mainly the events with a scattered angle (θ) larger than 90°. The formula for the Compton effect [Eq. (3)] indicates that the amount of energy deposited in the first interaction is larger than the remaining energy deposited in the second interaction position when the scattered angle is larger than 90°,

$$\frac{1}{E_S} - \frac{1}{E_0} = \frac{1}{\mathrm{m}_e\mathrm{c}^2}(1 - \cos\theta) \tag{3}$$

Here, E_0 corresponds to the initial energy of the incident photon, which is equivalent to 511 keV for an annihilation photon from positron decay. E_S is the amount of photon energy deposited at the second interaction position, and $\mathrm{m}_e\mathrm{c}^2$ is equivalent to the rest mass of an electron (511 keV).

2.C.2. Compton kinematics scheme

The Compton kinematics (CK) scheme selected a position which fitted Compton kinematics better as the first interacted position between S_1 and S_2.[22] For example, assuming S_1 as the first interacted position, scattered angle θ_{S_1} could be calculated in two different ways (Fig. 3). First, it could be calculated based on the geometrical positions of crystals in PET (θ_{G,S_1}).

$$\overrightarrow{PS_1} \cdot \overrightarrow{S_1S_2} = \left|\overrightarrow{S_1P}\right|\left|\overrightarrow{S_1S_2}\right| \cos\theta_{G,S_1} \tag{4}$$

Second, it could be calculated using the formula for the Compton effect (θ_{C,S_1}).

$$\frac{1}{E_{S_1}} - \frac{1}{E_{S_1} + E_{S_2}} = \frac{1}{\mathrm{m}_e\mathrm{c}^2}\left(1 - \cos\theta_{C,S_1}\right) \tag{5}$$

The angles θ_{G,S_2} and θ_{C,S_2} were calculated to be the same for S_2. Ideally, θ_G and θ_C are identical for the first interacted position, but the difference is not zero because of limited energy resolution and crystal size. Therefore, the position with a smaller difference between θ_G and θ_C was chosen as the first interacted one.

2.C.3. Neural network scheme

The neural network scheme (NN) consisted of training and test steps.[23] First, a network was trained with presimulated IDS events from a uniform phantom that had a size similar to the field of view. The network used in this study consisted of 4 input neurons in the input layer, 24 neurons in the hidden layer, and 2 outputs. The four inputs of the network were the deposited energies (E_{S_1},E_{S_2}) and scattered angles (θ_{G,S_1},θ_{G,S_2}) of S_1 and S_2 which characterized an IDS event (Fig. 3). While actual true LORs were given to the neural network, weights and biases of the hidden neurons were updated by Levenberg–Marquardt backpropagation to train the network to accurately choose true LORs. Second, the trained network was applied to the IDS test dataset. When the energies and the angles of each event were used as inputs, they passed through the hidden layer with optimized weights and biases. The outputs from the hidden layer passed through the sigmoid activation function which estimates probabilities that PS_1 and PS_2 were the true LORs. Finally, the LOR with a larger probability was chosen as the true LOR. All these procedures were conducted with the MATLAB (2017a) pattern recognition toolkit.

2.C.4. Proportional scheme

The proportional scheme (PR) was different from the other schemes that choose a single LOR among PS_1 and PS_2.[25] The main idea of the PR scheme was to distribute the IDS events that are proportionally weighted by the count of recorded double events for LORs. Total counts of LORs including IDS events were calculated as follows:

$$\begin{aligned} \mathrm{LOR}_{PS_1} &= D_{PS_1} + \frac{D_{PS_1}}{D_{PS_1} + D_{PS_2}} T_{PS_1S_2} \\ \mathrm{LOR}_{PS_2} &= D_{PS_2} + \frac{D_{PS_2}}{D_{PS_1} + D_{PS_2}} T_{PS_1S_2} \end{aligned} \tag{6}$$

where D and T represent the counts of doubles and triples assigned as IDS events, respectively. The subscripts indicate the positions involved in the events.

2.D. Scanner properties

We tested different energy resolutions and depth-of-interaction (DOI) layers in implementing the IDS recovery methods. To investigate the effects of energy resolution on recovery accuracy, 0%, 7%, 15%, and 20% were tested. The effects of the number of DOI layers were explored by testing one, two, and four DOI layers while the total crystal array length and energy resolution of 15% remained the same. Accuracy for crystal and DOI identification was assumed to be 100%.

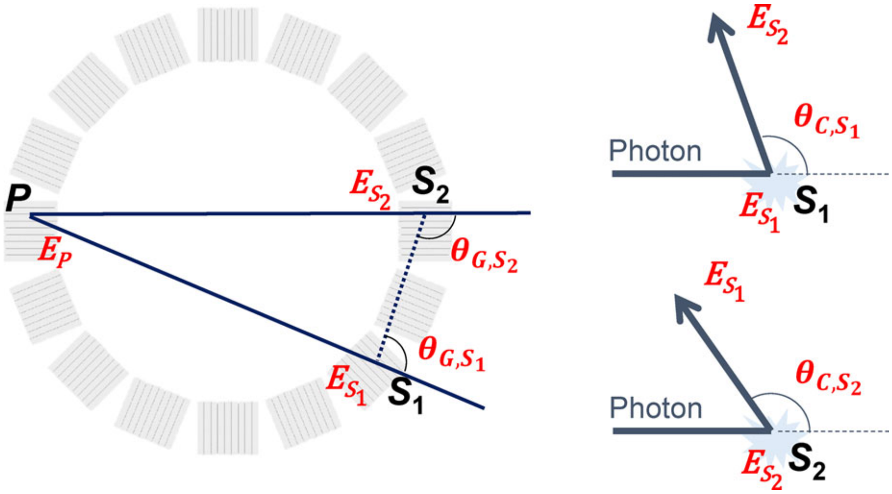

FIG. 3. Elements (energies and scattered angles) used in recovery schemes. [Color figure can be viewed at wileyonlinelibrary.com]

2.E. Reconstruction

It is important to perform individual normalizations of double events and triple events for accurate imaging.[25] Double and recovered IDS events were stored in separate histograms for the NEMA phantom and the cylindrical uniform phantom. Direct normalizations were applied to double data and recovered IDS data from the NEMA phantom using double and recovered IDS from the uniform phantom, respectively. Then, normalized double and IDS data were analytically added before the reconstruction.

The energy window of double coincidence was [250, 750] keV, which is practically used for small-animal PET, including SimPET. Random events and object scattered events were rejected from simulation outputs to observe only the effects of IDS. We implemented an ordered-subset expectation maximization method with four iterations (12 subsets) for the image reconstructions.

2.F. Performance evaluation and image analysis

The sensitivity increase and accuracy of IDS recovery were investigated as recovery performance. The sensitivity increase was defined as the number of recovered IDS events as a percentage of the number of existing double coincidence events acquired during the same time interval. Here, recovered IDS events are the events assigned as IDS and fell into the certain energy window specified in Section 2.B. An IDS event can be recovered either accurately, of which true LOR was chosen, or inaccurately, of which false LOR was chosen. To evaluate the abilities of IDS recovery methods choosing true LORs, accuracy was defined as a proportion of accurately recovered IDS events among the total recovered IDS events. Accuracy of 100% indicates that the IDS recovery method chose true LORs of every IDS event.

Reconstructed images of the NEMA phantom were analyzed in terms of mean pixel intensity, uniformity, SNR, contrast, and recovery coefficients. Mean pixel intensity (μ_{uni}) and uniformity (σ_{uni}) were calculated as mean and standard deviation (%), respectively, of pixel values inside the region of interest of the uniform region. SNR and contrast were measured with mean pixel values of hot (μ_{hot}) and cold (μ_{cold}) regions as follows:

$$\mathrm{SNR}_{\mathrm{hot}} = \frac{\mu_{\mathrm{hot}} - \mu_{\mathrm{uni}}}{\sigma_{\mathrm{uni}}}, \mathrm{SNR}_{\mathrm{cold}} = \frac{\mu_{\mathrm{uni}} - \mu_{\mathrm{cold}}}{\sigma_{\mathrm{uni}}} \tag{7}$$

$$\mathrm{Contrast}_{\mathrm{hot}} = \frac{\mu_{\mathrm{hot}} - \mu_{\mathrm{uni}}}{\mu_{\mathrm{uni}}}, \mathrm{Contrast}_{\mathrm{cold}} = \frac{\mu_{\mathrm{uni}} - \mu_{\mathrm{cold}}}{\mu_{\mathrm{uni}}}$$

The recovery coefficient was measured for the five rod regions. For each rod, the maximum pixel value of each transaxial slice was recorded in an axial line profile, and the μ_{rod} was calculated as the mean of this line profile.

$$\text{Recovery coefficient} = \frac{\mu_{\mathrm{rod}}}{\mu_{\mathrm{uni}}} \tag{9}$$

3. RESULTS

3.A. Valid IDS ratio

In our simulation setup, IDS occurred 3.6 times more frequently than RNT when energy criteria were not applied. As shown in Table II, the valid IDS ratio previously defined in the Section 2.B is highly dependent on the energy window. A narrower energy window is more likely to reject RNT events and correctly assign the LOR candidates of IDS events. The valid IDS ratio increased nearly 10% when RNT events were fully excluded by random correction. This indicates that the 10% of RNT events were wrongly assigned as IDS. When we exclude RNT events, almost 100% of IDS events was correctly assigned in energy windows of [350, 650] and [450, 550] keV.

3.B. Energy window and recovery scheme

3.B.1. *Performance evaluation*

By utilizing recovered IDS events, sensitivity increased by 33%, 24%, and 17% for energy windows [250, 750] keV,

TABLE II. Valid IDS ratio depending on energy window.

Energy window	[250, 750] keV (%)	[350, 650] keV (%)	[450, 550] keV (%)
RNT included	63.43	85.40	89.84
RNT excluded	74.91	98.06	99.84

[350, 650] keV, and [450, 550] keV, respectively, compared to sensitivity using double coincidences only (Table III). A broader energy window yielded a larger sensitivity increase because a larger number of IDS events met the energy criteria specified in the Section 2.B. Sensitivity increase was same regardless of the recovery schemes because the recovery scheme does not affect assigning IDS event.

Accuracy increased as the energy window narrowed for all schemes in common (Table III). The first reason was that the higher energy threshold rejects IDS events in which one or both annihilation photons escape after scattering in the detector. In the processing of these events, scattered angles ($\theta_{S_1}, \theta_{S_2}$) were wrongly calculated due to insufficient deposition of energies. Second, a low-energy threshold of [250, 750] keV contained the events in which a single photon underwent two Compton scatters in the different detector blocks and detected coincidently. This type of event was counted as a valid IDS according to our energy criteria although it was not an actual IDS event we wanted to recover. Lastly, when a low threshold of the wide energy window was applied, the events with lower energies were more likely to be imprecise in energy measurement because PET has worse energy resolution in lower energy ranges.

When we compared the recovery schemes, accuracy was in the order of NN, CK, and ME. Because the neural network works well in overall medical uses, NN showed the best performance in choosing true LORs and yielded nearly 10% higher accuracy than CK and ME.[33,34] For the PR scheme, we cannot define its accuracy because it does not choose a single LOR as a true one but adds the probabilities of true LORs determined by double coincidence distribution to both LORs. Therefore, the accuracy of the PR scheme was not measured in this study.

3.B.2. Image analysis — energy window

Figure 4 shows the reconstructed images obtained with various energy windows after recovering IDS with the NN scheme. The wider energy window of IDS events yielded brighter images because of a larger increase in sensitivity. In addition, IDS recovered images with wider energy windows had smaller statistical noise level and better SNR. All recovery schemes showed the identical tendency (Fig. 5). When the same energy window was applied, the mean pixel intensity, standard deviation, and SNR were comparable for all the schemes because of the same sensitivity increase.

TABLE III. Sensitivity increase and accuracy of IDS recovery methods.

Energy window (keV)	Sensitivity increase (%)	Accuracy (%)		
		ME	CK	NN
[250, 750]	33.23	48.39	52.76	63.95
[350, 650]	24.11	59.03	58.30	68.63
[450, 550]	17.43	59.04	59.47	69.11

On the contrary, contrast and recovery coefficients were better for a narrower energy window, which yielded higher accuracy because quantitative accuracy and spatial resolution of images are affected by IDS recovery accuracy (Figs. 5 and 6). Narrower energy windows included fewer false LORs, which degrade images.

3.B.3. Image analysis — recovery scheme

Comparing ME, CK, and NN schemes, SNR, contrast, and recovery coefficients were better in the scheme with higher accuracy (Figs. 5 and 6). These results indicate that reducing false LORs improves image quality. Figure 7 shows the reconstructed images of using different recovery schemes with the same IDS energy window [350, 650] keV. The images of hot and cold regions reflected the relationship between the accuracy of IDS recovery and image quality.

The PR scheme showed a better contrast and recovery coefficient compared with other IDS recovery schemes (Figs. 5 and 6). It also produced the largest increase of pixel intensities in hot region and rods, as shown in the profiles of Fig. 7. These imply that the PR scheme yields the best image quality with the smallest error in positioning the LORs of IDS events.

Effects of recovery schemes on the reduction in acquisition time are shown in Fig. 8. Schemes with higher accuracy yielded better SNR at each acquisition time point because they accurately positioned the LORs passing through the ROIs. Therefore, they required less time to achieve the same SNR level to image without IDS recovery acquired for 10 min. For the PR scheme, time reduction of 20% was acceptable, which agrees with previously reported results.[25]

3.C. Performance dependence on scanner properties

3.C.1. Energy resolution

Energy resolution was related to the number of IDS events that fall into a certain energy window. Figure 9(a) shows the effect of energy resolution on sensitivity for all the schemes in common. The number of assigned IDS events for [450, 550] keV largely decreased when energy uncertainties increased because a large proportion of events with actual energy of 511 keV were rejected. For broader energy windows, loss of sensitivity due to energy uncertainty was insignificant because the entire events of a 511-keV peak fell into the energy windows.

Energy resolution was also an important factor for recovery accuracy because many schemes use energy information for the recovery. For most of the methods, recovery accuracy

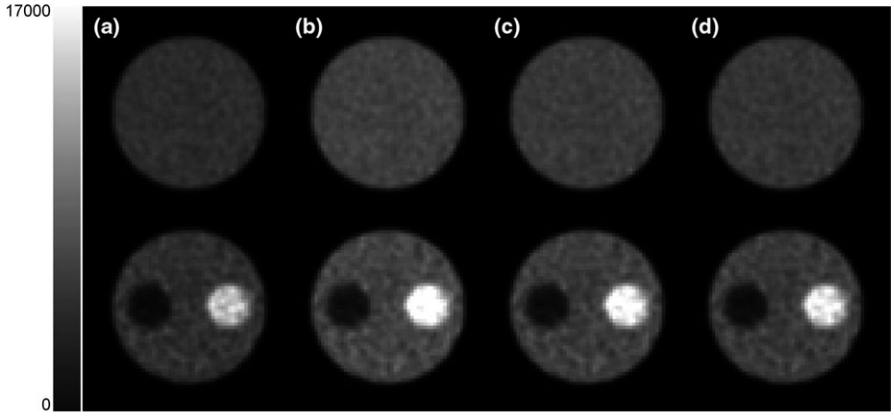

FIG. 4. Reconstructed images of uniform region (top) and hot/cold region (bottom) with NN scheme applied. (a) Without IDS recovery, (b) [250, 750] keV, (c) [350, 650] keV, and (d) [450, 550] keV.

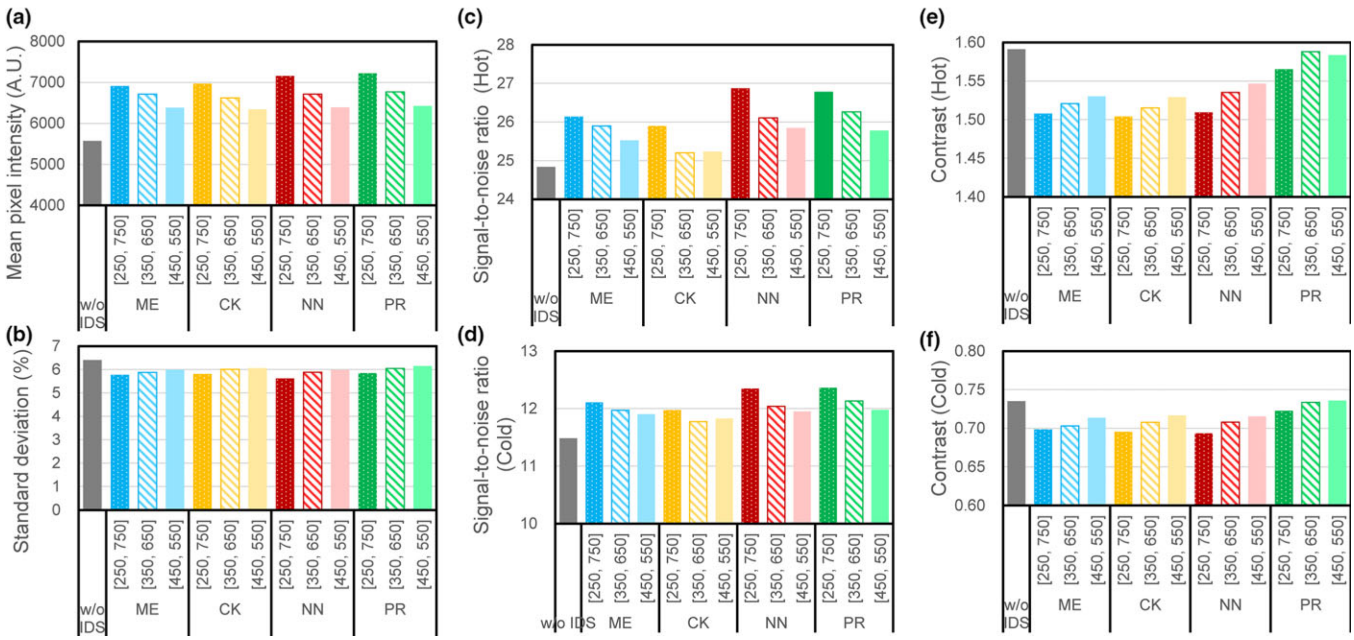

FIG. 5. Quality of IDS recovered images. (a) Mean pixel intensity and (b) standard deviation measured at the uniform region. (c), (d) SNR and (e), (f) contrast measured at the hot and cold regions. [Color figure can be viewed at wileyonlinelibrary.com]

decreased with increasing energy uncertainties [Fig. 9(b)]. The ME scheme was the most robust to the degradation of energy resolution. CK was the most sensitive to energy resolution because energy values directly affect the calculations of scatter angles (θ_C). Specifically, in the case of [350, 650] keV, CK was even worse than the ME scheme when energy resolution was worse than 15%. The NN scheme was also affected by energy resolution because the energies were used as inputs of the network. When ideal energy resolution of 0% was achieved in our system and energy window of [350, 650] keV was applied, the accuracies increased by 0.53%, 3.49% and 1.98% for ME, CK, and NN schemes, respectively, compared with the more realistic energy resolution of 15%. Meanwhile, the PR scheme was excluded in this section because it does not require any energy information for recovery.

3.C.2. DOI layers

The DOI capability was expected to be another important factor for recovery accuracy because it provides precise information of interaction position, which leads to accurate calculation of Compton scatter angle.[35,36] When DOI positioning is assumed to be perfectly accurate, IDS recovery accuracy improved with increasing number of DOI layers for CK and NN schemes (Fig. 10). These are the schemes that use scatter angles calculated from geometrical relationships between interacted crystals. Expanding the number of DOI layers increased the accuracy by approximately 5% in most methods. However, the limitations on position uncertainty still existed due to intercrystal scatter, which occurs by one or more Compton scatters of a photon within a detector block and leads to incorrect positioning of the interacted crystal.

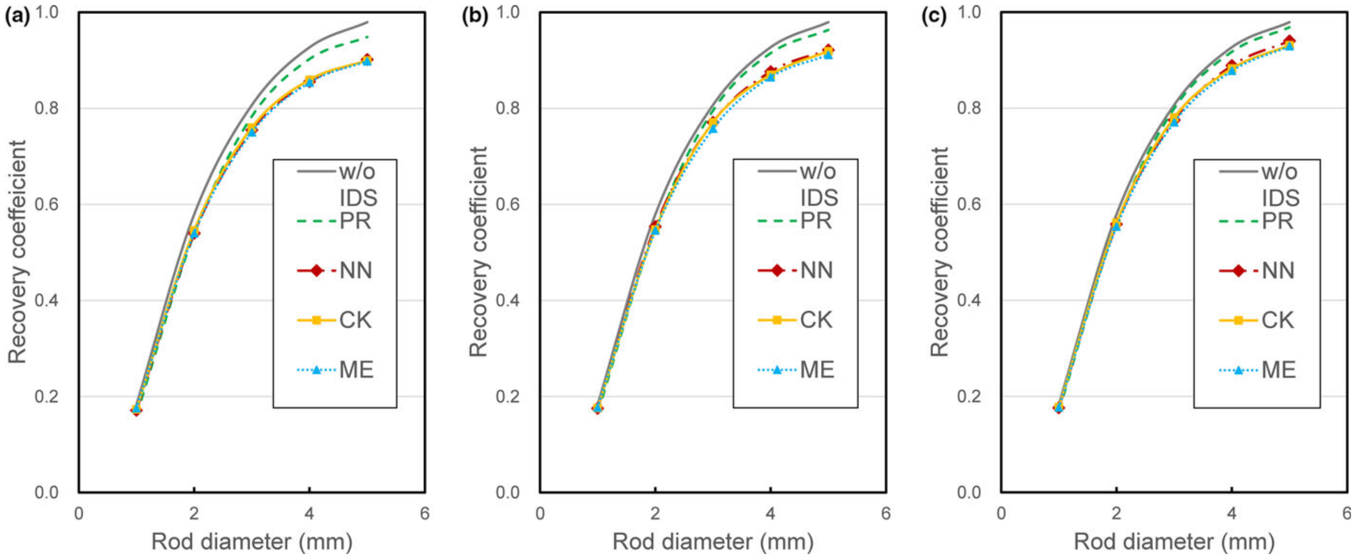

FIG. 6. Recovery coefficients measured at the rod region with applying energy window of (a) [250, 750] keV, (b) [350, 650] keV, and (c) [450, 550] keV. [Color figure can be viewed at wileyonlinelibrary.com]

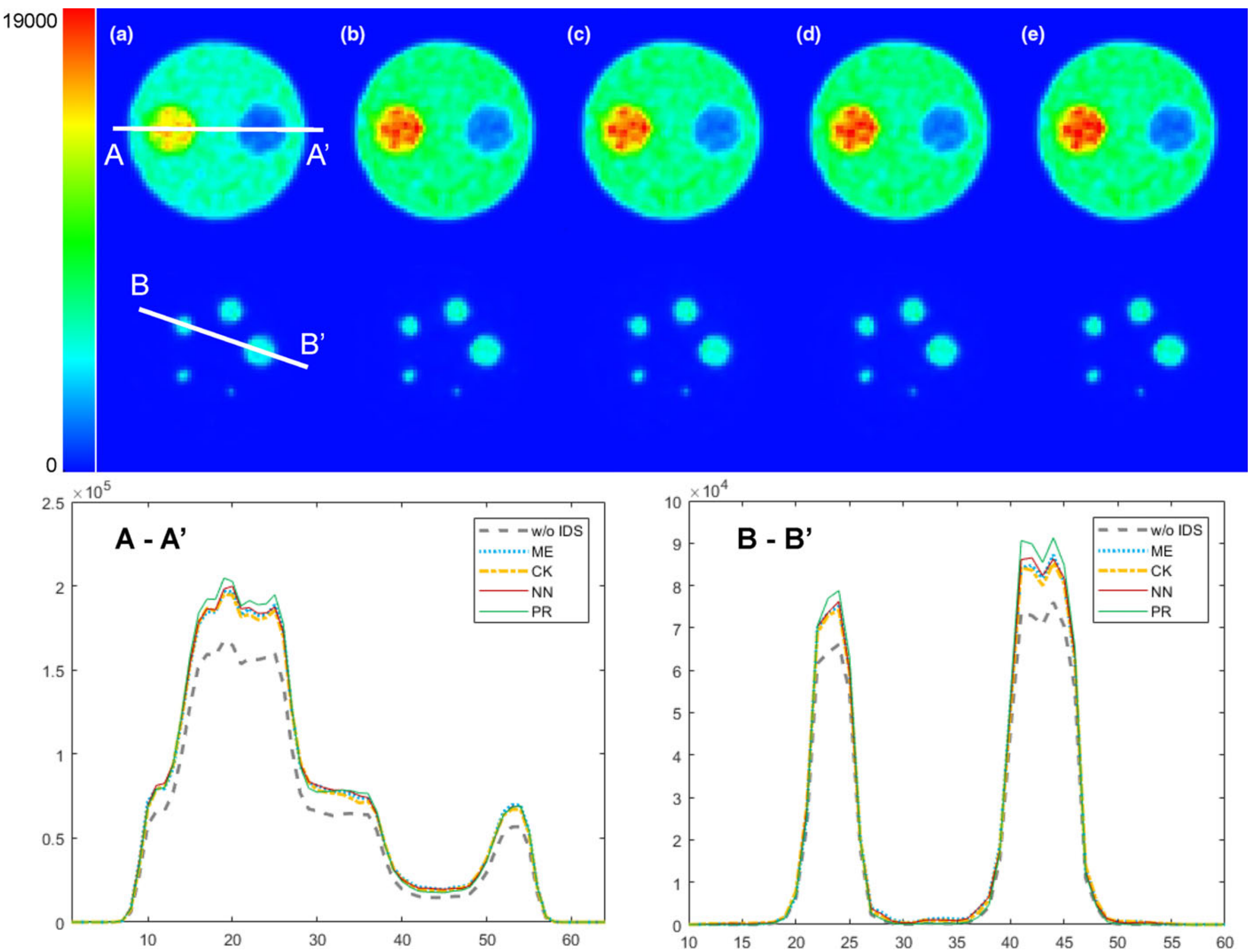

FIG. 7. (Top) Reconstructed images of hot/cold region and rod region with applications of (a) without IDS, (b) ME, (c) CK, (d) NN, and (e) PR schemes. (bottom) Projected line profile along A–A′ of hot/cold region and B–B′ of rod region. Energy window of [350, 650] keV was applied in common. [Color figure can be viewed at wileyonlinelibrary.com]

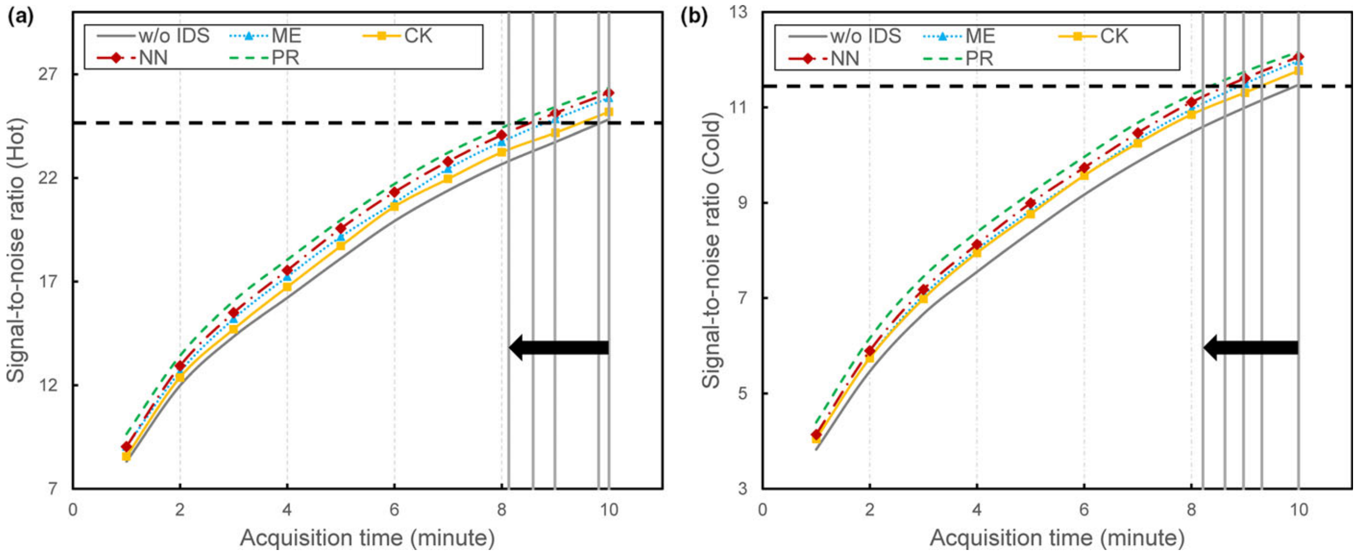

FIG. 8. SNR of (a) hot and (b) cold region over acquisition time. Energy window of [350, 650] keV was applied in common. [Color figure can be viewed at wileyonlinelibrary.com]

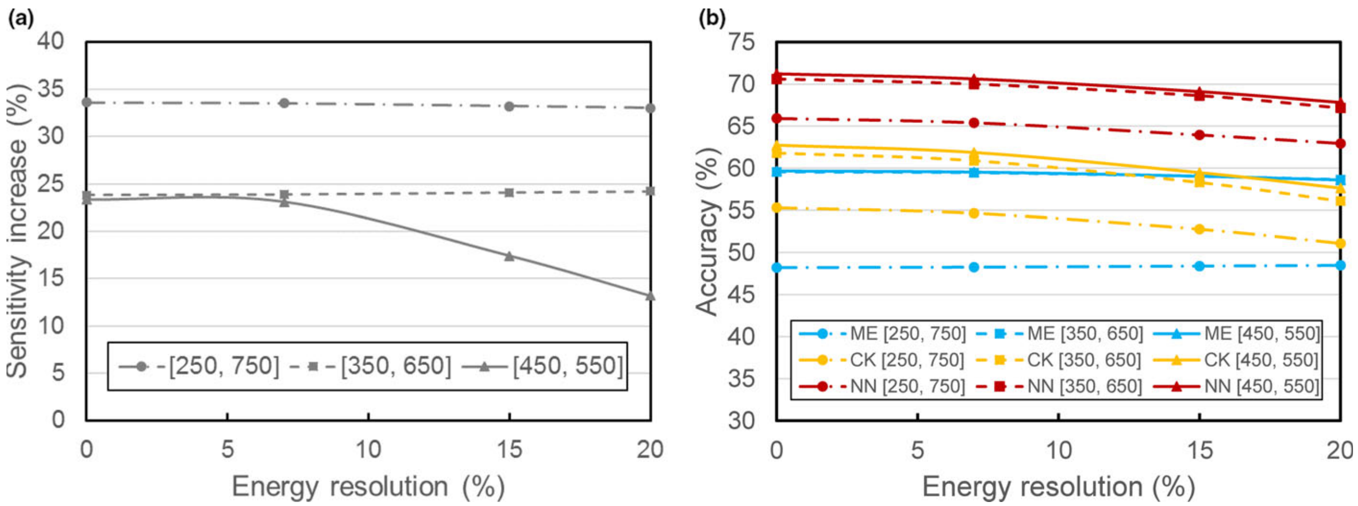

FIG. 9. (a) Sensitivity increase and (b) accuracy of IDS recovery methods' dependence on energy resolution. [Color figure can be viewed at wileyonlinelibrary.com]

For the ME scheme, there was no difference in accuracy with a different number of DOI layers because it did not require interaction positions for recovery.

4. DISCUSSION

The valid IDS ratio that is related to correct assignment of IDS events was affected by the width of the energy window. Sensitivity increase depended on energy window and energy resolution, while accuracy was dependent on the energy window, recovery scheme, energy resolution, and number of DOI layers. An energy window of [350, 650] keV for assigning triple coincidence as IDS event seems to be appropriate for small-animal PET scanners because it achieves a large increase in sensitivity with a recovery accuracy comparable to [450, 550] keV. We observed correlations between performance and effects on the image quality of the IDS recovery methods. In image quality analysis, sensitivity increase was especially critical to overall pixel intensity, uniformity, and SNR due to effects on noise reduction. When the same energy window was applied, schemes with higher accuracy tended to yield better image quality, especially contrast and recovery coefficients because fewer false LORs were included. By applying IDS recovery, contrast and recovery coefficients were degraded compared to the non-IDS-recovered images, especially for ME and CK schemes. However, the degradation was less than 7% in each case, and the advantages in scan time and dose reduction would overcome this degradation in practical PET imaging. In case of the PR scheme, which differs from other schemes in its LOR selection algorithm, it yielded the best image quality and the largest reduction in scan time. Although we did not reconstruct

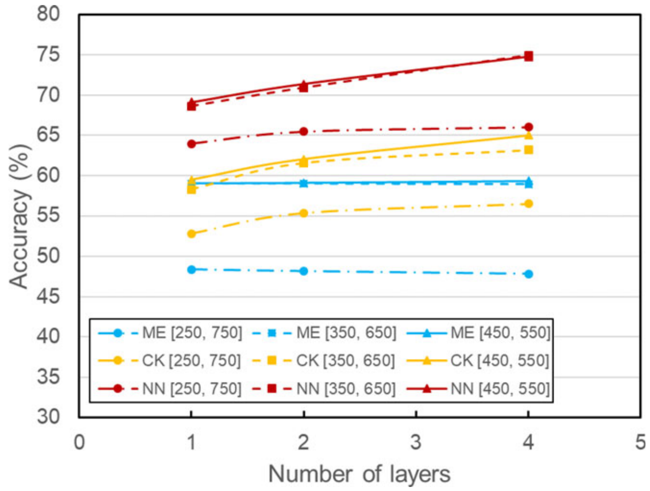

FIG. 10. Accuracy of IDS recovery methods dependence on number of DOI layers. [Color figure can be viewed at wileyonlinelibrary.com]

images and analyze image quality for every combination of PET scanner energy resolution and DOI capability in this work, it is possible to predict the image quality in each case based on the tendencies observed in this study.

Importantly, the differences in image quality using different IDS recovery methods were not very remarkable despite different recovery accuracies. Defining the positions of interacted crystals using transaxial and axial indices, as described in Fig. 11(a), the differences in indices between the points involved in a true LOR [PS_1 in Fig. 11(a)] and a scattered photon [S_1S_2 in Fig. 11(a)] in IDS events from the uniform phantom were recorded, respectively. The histograms in Fig. 11(b) show that most of the Compton-scattered photons in IDS events interact with very near crystals that have index differences less than 10, while true LORs are usually positioned across the center region of the field of view. Photons with lower energy have a larger cross section of photoelectric absorption in scintillation crystals, and thus have a greater chance to interact over a short travel path. Therefore, a large proportion of the falsely recovered LORs is placed near the true LORs and consequently causes only a minor degradation of image quality.

Because this work was completely conducted by simulation, there are several further issues to be considered to implement IDS recovery in reality. First, signal readout from individual detector blocks is required to take full advantage of the sensitivity increase. When a number of detector blocks are multiplexed as a single module, IDS events that occurred within the module are not recognized as IDS and, therefore, not utilized for the recovery. It is even more important because a large proportion of IDS events occur between adjacent detector blocks. Moreover, crystals with which photons interact have to be correctly identified to enhance image quality with IDS recovery. Contrary to the simulation condition, crystal identifying error would arise not only from multiplexing and light sharing but also from low energies of IDS events. Events with small energies have higher position uncertainties in crystal flood maps.

The selection of IDS recovery scheme involves further consideration due to its intrinsic characteristics of recovery principles. Various schemes evaluated in this study used detected energies and positions for recovery. Therefore, accuracy was highly affected by preciseness of information

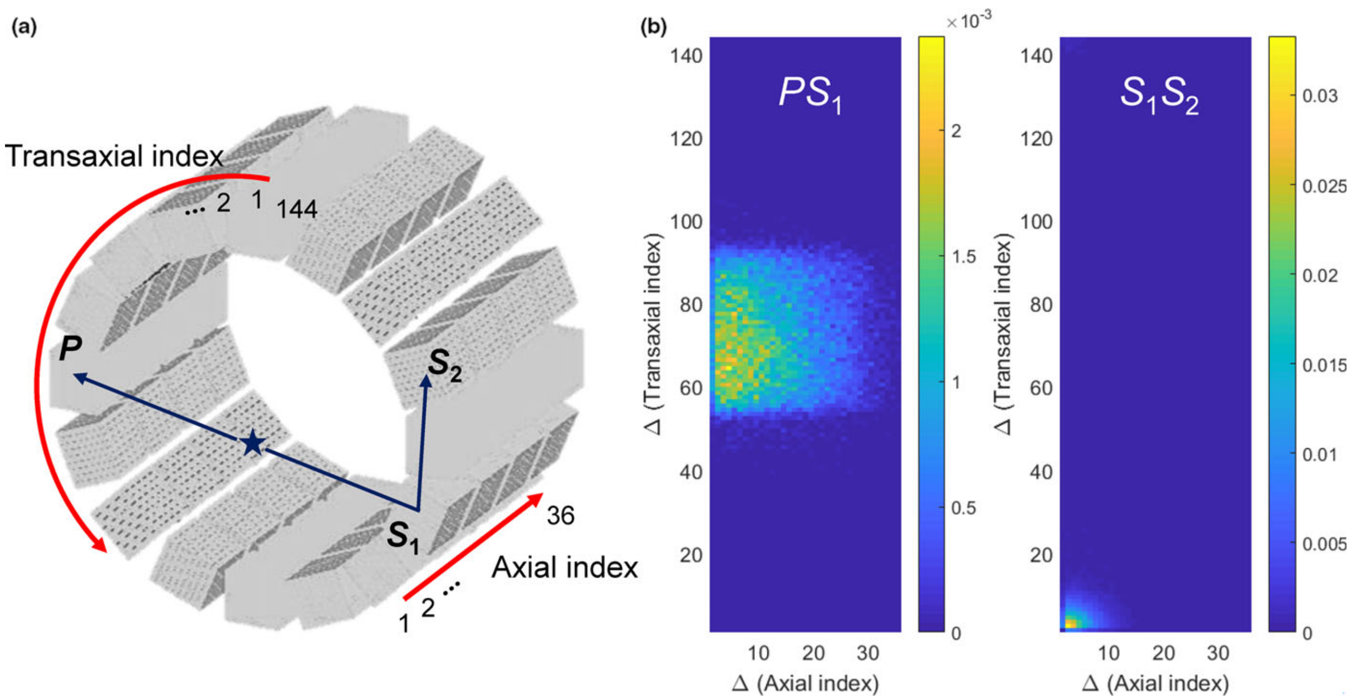

FIG. 11. Distribution of IDS events in the PET scanner. (a) Indexing the crystals along transaxial and axial directions. (b) Probability distribution histograms of difference in crystal indices involved in true LOR and LOR drawn by scattered photon of IDS events. [Color figure can be viewed at wileyonlinelibrary.com]

measured by the PET scanner, as shown in Section 3.C. Better energy resolution and DOI capability for PET would achieve a higher accuracy of ME, CK, and NN schemes. For the PR scheme, both energy resolution and DOI capability are not critical factors determining its performance because it does not require energy and position information.

Processing capability of IDS events is another factor to be considered. First, the coincidence module in PET data acquisition has to sort triple coincidences accurately. Simple schemes such as ME and PR, which use simple comparison of energies and the number of double coincidences stored in the histogram, respectively, do not require computational complexities of processing units when being implemented in a real system. The CK and NN schemes require calculation of scatter angle using the formula of Compton kinematics and vectors of crystal positions. The NN scheme further requires calculations in a network trained by simulation data. However, it is reported that the computational burden of the NN scheme is manageable, even in existing PET systems.[24]

Based on the findings of this work, we look forward to implementing IDS recovery in our real PET system and establishing the proper method to maximize the efficiency. We will also investigate the applicability of the IDS recovery method further by performing phantom and animal studies.

5. CONCLUSIONS

In this work, we simulated IDS recovery in a small-animal PET scanner by applying different factors to evaluate their effects on sensitivity increase, recovery accuracy, and quality of reconstructed phantom images. Sensitivity increase was highly dependent on the energy window and energy resolution, while recovery accuracy was affected by all the factors. In image quality analysis, sensitivity increase and recovery accuracy dominantly affected noise and quantitative accuracy, respectively. Among the recovery schemes, the PR scheme obtained the best image quality. The results would provide useful guidelines for implementation of IDS recovery in real PET scanners.

ACKNOWLEDGMENTS

This work was supported by grants from the National Research Foundation of Korea (NRF) funded by the Korean Ministry of Science and ICT (Grant Nos. NRF-2014M3C7034000 and NRF-2016R1A2B3014645).

CONFLICTS OF INTEREST

The authors have no conflicts to disclose.

[a]Author to whom correspondence should be addressed. Electronic mail: jaes@snu.ac.kr; Telephone: +82 2 2072 2938; Fax: +82 2 745 2938.

REFERENCES

1. Cherry SR, Shao Y, Silverman RW, et al. MicroPET: a high resolution PET scanner for imaging small animals. *IEEE Trans Nucl Sci*. 1997;44:1161–1166.
2. Phelps ME. Positron emission tomography provides molecular imaging of biological processes. *Proc Natl Acad Sci USA*. 2000;97:9226–9233.
3. Ahn B-C. Nuclear medicine in the era of precision medicine. *Nucl Med Mol Imaging*. 2017;51:99–100.
4. Eriksson L, Townsend D, Conti M, et al. An investigation of sensitivity limits in PET scanners. *Nucl Instrum Methods Phys Res A*. 2007;580:836–842.
5. Borasi G, Fioroni F, Del Guerra A, Lucignani G. PET systems: the value of added length. *Eur J Nucl Med Mol Imaging*. 2010;37:1629–1632.
6. Surti S, Werner ME, Karp JS. Study of PET scanner designs using clinical metrics to optimize the scanner axial FOV and crystal thickness. *Phys Med Biol*. 2013;58:3995–4012.
7. Isnaini I, Obi T, Yoshida E, Yamaya T. Monte Carlo simulation of efficient data acquisition for an entire-body PET scanner. *Nucl Instrum Methods Phys Res A*. 2014;751:36–40.
8. Zhang X, Zhou J, Cherry SR, Badawi RD, Qi J. Quantitative image reconstruction for total-body PET imaging using 2-meter long EXPLORER scanner. *Phys Med Biol*. 2017;62:2465–2485.
9. Poon JK, Dahlbom ML, Moses WW, et al. Optimal whole-body PET scanner configurations for different volumes of LSO scintillator: a simulation study. *Phys Med Biol*. 2012;57:4077–4094.
10. El Fakhri G, Surti S, Trott CM, Scheuermann J, Karp JS. Improvement in lesion detection with whole-body oncologic time-of-flight PET. *J Nuc Med*. 2011;52:347–353.
11. Karp JS, Surti S, Daube-Witherspoon ME, Muehllehner G. Benefit of time-of-flight in PET: experimental and clinical results. *J Nuc Med*. 2008;49:462–470.
12. Son J-W, Ko GB, Won JY, Yoon HS, Lee JS. Development and performance evaluation of a time-of-flight positron emission tomography detector based on a high-quantum-efficiency multi-anode photomultiplier tube. *IEEE Trans Nucl Sci*. 2016;63:44–51.
13. Conti M. Improving time resolution in time-of-flight PET. *Nucl Instrum Methods Phys Res A*. 2011;648:S194–S198.
14. Ko GB, Lee JS. Performance characterization of high quantum efficiency metal package photomultiplier tubes for time-of-flight and high-resolution PET applications. *Med Phys*. 2015;42:510–520.
15. Cates JW, Levin CS. Advances in coincidence time resolution for PET. *Phys Med Biol*. 2016;61:2255–2264.
16. Chinn G, Foudray AMK, Levin CS. A method to include single photon events in image reconstruction for a 1 mm resolution PET system built with advanced 3-D positioning detectors. *IEEE Nucl Sci Symp Conf Rec*. 2006:1740–1745.
17. Levin CS. New imaging technologies to enhance the molecular sensitivity of positron emission tomography. *Proc IEEE*. 2008;96:439–467.
18. Yoshida E, Tashima H, Levin CS, Parodi K, Yamaya T. Simulation study of a DOI-based PET-Compton imaging system for positron emitters. *IEEE Nucl Sci Symp Conf Rec*. 2015. https://doi.org/10.1109/NSSMIC.2015.7582080.
19. Cal-González J, Lage E, Herranz E, et al. Simulation of triple coincidences in PET. *Phys Med Biol*. 2015;60:117–136.
20. Wagadarikar AA, Ivan A, Dolinsky S, McDaniel DL. Sensitivity improvement of time-of-flight (ToF) PET detector through recovery of Compton scattered annihilation photons. *IEEE Trans Nucl Sci*. 2014;61:121–125.
21. Comanor KA, Virador PRG, Moses WW. Algorithms to identify detector Compton scatter in PET modules. *IEEE Trans Nucl Sci*. 1996;43:2213–2218.
22. Rafecas M, Böning G, Pichler BJ, Lorenz E, Schwaiger M, Ziegler SI. Inter-crystal scatter in a dual layer, high resolution LSO-APD positron emission tomograph. *Phys Med Biol*. 2003;48:821–848.
23. Michaud J-B, Tétrault M-A, Beaudoin J-F, et al. Sensitivity increase through a neural network method for LOR recovery of ICS triple coincidences in high-resolution pixelated detectors PET scanners. *IEEE Trans Nucl Sci*. 2015;62:82–94.
24. Lage E, Parot V, Moore SC, et al. Recovery and normalization of triple coincidences in PET. *Med Phys*. 2015;42:1398–1410.

25. Shao Y, Cherry SR, Siegel S, Silvermann RW. A study of inter-crystal scatter in small scintillators arrays designed for high resolution PET imaging. *IEEE Trans Nucl Sci*. 1996;43:1938–1944.
26. Michaud J-B, Brunet C-A, Rafecas M, Lecomte R, Fontaine R. Sensitivity in PET: neural networks as an alternative to Compton photons LOR analysis. *IEEE Nucl Sci Symp Conf Rec*. 2007:3594–3600.
27. Pratx G, Levin CS. Bayesian reconstruction of photon interaction sequences for high-resolution PET detectors. *Phys Med Biol*. 2009;54: 5073–5094.
28. Gillam JE, Solevi P, Oliver JF, et al. Sensitivity recovery for the AX-PET prototype using inter-crystal scattering events. *Phys Med Biol*. 2014;59:4065–4083.
29. Jan S, Santin G, Strul D, et al. GATE: a simulation toolkit for PET and SPECT. *Phys Med Biol*. 2004;49:4543–4561.
30. Ko GB, Kim KY, Yoon HS, et al. Evaluation of a silicon photomultiplier PET insert for simultaneous PET and MR imaging. *Med Phys*. 2016;43:72–83.
31. Ko GB, Yoon HS, Kim KY, et al. Simultaneous multiparametric PET/MRI with silicon photomultiplier PET and ultra-high-field MRI for small-animal imaging. *J Nucl Med*. 2016;57:1309–1315.
32. NEMA standards publication NU 4-2008. *Performance measurements for small animal positron emission tomographs*. Rosslyn, VA: National Electrical Manufacturers Association; 2008.
33. Mohammadi MR, Khaleghi A, Nasrabadi AM, Rafieivand S, Begol M, Zarafshan H. EEG classification of ADHD and normal children using non-linear features and neural network. *Biomed Eng Lett*. 2016;6:66–73.
34. Yoo Y. On predicting epileptic seizures from intracranial electroencephalography. *Biomed Eng Lett*. 2017;7:1–5.
35. Ito M, Hong SJ, Lee JS. Positron emission tomography (PET) detectors with depth-of-interaction (DOI) capability. *Biomed Eng Lett*. 2011;1:70–81.
36. Lee MS, Kim KY, Ko GB, Lee JS. Prototype pre-clinical PET scanner with depth-of-interaction measurements using single-layer crystal array and single-ended readout. *Phys Med Biol*. 2017;62:3983–3996.